

Learning Content-enhanced Mask Transformer for Domain Generalized Urban-Scene Segmentation

Qi Bi Shaodi You Theo Gevers
 Computer Vision Research Group
 University of Amsterdam
 Amsterdam, 1098 XH, The Netherlands
 {q.bi, s.you, th.gevers}@uva.nl

Abstract

Domain-generalized urban-scene semantic segmentation (USSS) aims to learn generalized semantic predictions across diverse urban-scene styles. Unlike domain gap challenges, USSS is unique in that the semantic categories are often similar in different urban scenes, while the styles can vary significantly due to changes in urban landscapes, weather conditions, lighting, and other factors. Existing approaches typically rely on convolutional neural networks (CNNs) to learn the content of urban scenes.

In this paper, we propose a Content-enhanced Mask TransFormer (CMFormer) for domain-generalized USSS. The main idea is to enhance the focus of the fundamental component, the mask attention mechanism, in Transformer segmentation models on content information. To achieve this, we introduce a novel content-enhanced mask attention mechanism. It learns mask queries from both the image feature and its down-sampled counterpart, as lower-resolution image features usually contain more robust content information and are less sensitive to style variations. These features are fused into a Transformer decoder and integrated into a multi-resolution content-enhanced mask attention learning scheme.

Extensive experiments conducted on various domain-generalized urban-scene segmentation datasets demonstrate that the proposed CMFormer significantly outperforms existing CNN-based methods for domain-generalized semantic segmentation, achieving improvements of up to 14.00% in terms of mIoU (mean intersection over union). The source code for CMFormer will be made available at this repository.

1 Introduction

Urban-scene semantic segmentation (USSS) is a challenging problem because of the large scene variations due to changing landscape, weather, and lighting conditions [44, 31, 10, 4]. Unreliable USSS can pose a significant risk to road users. Hence, domain generalization is essential for robust USSS [35, 16, 7]. In contrast to common domain generalization, domain generalized USSS requires special attention because the domain gap is mainly caused by large style variations whereas changes in semantics largely remain consistent (see Fig. 1 for an example).

Existing approaches can be divided into two groups. One group focuses on the style de-coupling. This is usually achieved by a normalization [35, 16, 38] or whitening [36, 7, 57, 38] transformation. However, the de-coupling methodology falls short as the content is not learnt in a robust way. The other group is based on adverse domain training [65, 23, 66]. However, these methods usually do not particularly focus on urban styles and therefore their performance is limited.

In this paper, we focus on two main objectives for USSS: (1) a concise but expressive representation of the content, and (2) a robust module for style change handling. For the first goal, we propose to use

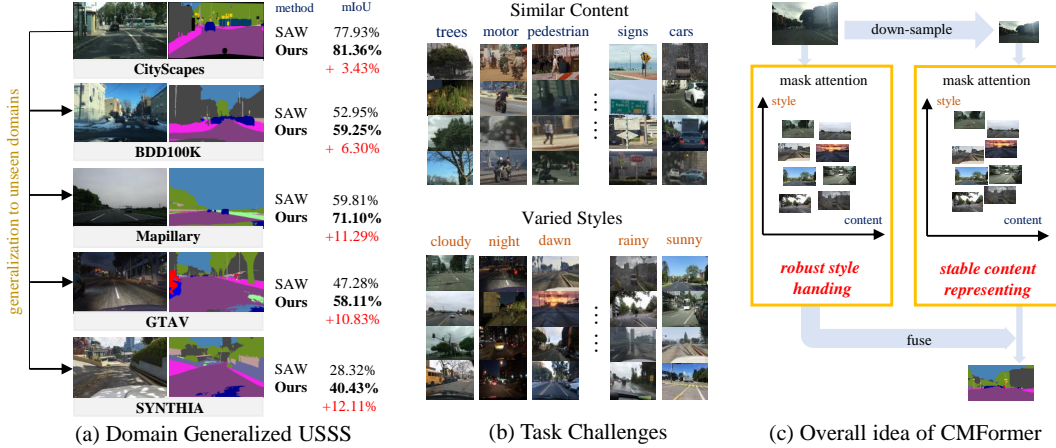


Figure 1: (a) Example of domain generalized USSS (top: source domain, rest: target domain); (b) The key challenge lies in the domain gap is mainly from the extremely-varied styles but the content is similar; (c) The proposed CMFormer with content-enhanced mask attention focus on: 1) learn an expressive content representation, 2) robust to style variation. SAW: the present state-of-the-art [38].

Mask Transformer. Transformer segmentation models [47, 5, 51, 60, 61, 6] provide more expressive representations than CNN-based methods because of their mask attention mechanisms allowing to incorporate long-range dependencies [27, 28, 11], context [19], and saliency [5, 6]. For the second goal, mask-level learning is used which is less sensitive than pixel-level learning in handling style changes [34, 12, 52].

To this end, a novel **Content-enhanced Mask TransFormer (CMFormer)** is proposed. Particularly, a content-enhanced mask attention mechanism is introduced, which takes the original image feature together with its down-sampled counterpart as input. The down-sampled features contain more content and are less sensitive to style variations. Both features are fused to learn the context. Then, the content-enhanced mask attention is extended to incorporate multi-resolution features.

Large-scale experiments are conducted with various domain generalized USSS settings, *i.e.*, trained on one dataset from [42, 43, 8, 33, 59] as the source domain, and validated on the rest of the four datasets as the unseen target domains. The experiments show that the proposed CMFormer achieves upto 14.00% mIoU improvement compared to the state-of-the-art (*e.g.*, SAW [38], WildNet [23]). The proposed CMFormer also outperforms existing mask-level Transformer segmentation methods and the generic segmentation methods pre-trained by the foundation model (*i.e.*, SAM [21], SegGPT [54]). It also shows state-of-the-art performance on synthetic-to-real and ideal-to-adverse generalization.

Our contribution is summarized as follows:

- To the best of our knowledge, it is the first attempt to use ViT for the task of domain generalized USSS.
- A content-enhanced mask attention mechanism is proposed enhancing the content information from image features.
- A multi-resolution content-enhanced mask attention learning scheme is proposed for expressive content representation and style robustness.
- Extensive experiments show a large performance improvement over existing SOTA by upto 14.00% mIoU.

2 Related Work

Domain Generalization has been studied on no task-specific scenarios in the field of both machine learning and computer vision. Harary *et al.* [13] considered domain generalization in an unsupervised manner by learning a *domain bridge*. Hu *et al.* [15] proposed a framework for image retrieval in an unsupervised setting. Zhou *et al.* [67] proposed a framework to generalize to new homogeneous domains. Qiao *et al.* [41] and Peng *et al.* [39] proposed to learn domain generalization from a single source domain. Many other methods have been proposed such as entropy regularization [64],

casual matching [29], extrinsic-intrinsic interaction [53], balance invariance [2], batch normalization embeddings [45] and multiple latent domain modeling [30].

Domain Generalized Semantic Segmentation can be regarded as the exploration of the prior unsupervised domain adaption segmentation task [38, 37, 63], but requires a larger generalization capability of a model on a variety of target domains. Existing methods focus on the generalization of in-the-wild [40], scribble [48] and multi-source images [20, 22], where substantial alterations can occur in both the content and style.

Domain Generalized USSS focuses on the generalization of driving-scenes [8, 59, 33, 43, 42]. These methods use either a normalization transformation (*e.g.*, IBN [35], IN [16], SAN [38]) or whitening transformation (*e.g.*, IW [36], ISW [7], DURL [57], SAW [38]) on the training domain, to enable the model to generalize better on the target domains. Other advanced methods for domain generalization in segmentation typically rely on external images to incorporate more diverse styles [23, 65, 66, 25], and leverage content consistency across multi-scale features [62]. To the best of our knowledge, all of these methods are based on CNN.

Mask Transformer for Semantic Segmentation Earlier ViT based segmentation models (*e.g.*, SegFormer [56]) follow the CNN based pipeline. Recently, the focus is on mask-level pipelines, which use the queries in the Transformer decoder to learn the masks, *e.g.*, Segmenter [47], MaskFormer [5], Max-DeepLab [51], CMT-DeepLab [60], kMaX-DeepLab [61] and *etc.* More recently, Mask2Former [6] further simplified the pipeline of MaskFormer and achieves better performance.

3 Methodology

3.1 Problem Definition

Domain Generalization can be formulated as a worst-case problem [24, 66, 50]. Given a source domain \mathcal{S} , and a set of unseen target domains $\mathcal{T}_1, \mathcal{T}_2, \dots$, a model parameterized by θ with the task-specific loss \mathcal{L}_{task} , the generic domain generalization task can be formulated as a worst-case problem, given by

$$\min_{\theta} \sup_{\mathcal{T}: D(\mathcal{S}; \mathcal{T}_1, \mathcal{T}_2, \dots) \leq \rho} \mathbb{E}_T[\mathcal{L}_{task}(\theta; \mathcal{T}_1, \mathcal{T}_2, \dots)], \quad (1)$$

where θ denotes the model parameters, $D(\mathcal{S}; \mathcal{T}_1, \mathcal{T}_2, \dots)$ corresponds to the distance between the source \mathcal{S} and target domain \mathcal{T} , and ρ denotes the constraint threshold.

Domain generalized USSS is challenging as it has similar content (*e.g.*, semantics) but variation of style (*e.g.*, urban landscapes, weather, season, illumination) among each domain $\mathcal{S}, \mathcal{T}_1, \mathcal{T}_2, \dots$. Visual examples have been provided in Fig. 1. Here we analyze the feature domain. As shown in Fig. 2a, while the content distribution is similar, the style distribution is separated and accounts for the domain gap. Our goal is to find a representation where both style and content are similarly distributed among domains, therefore minimizing the domain gap (in Fig. 2b).

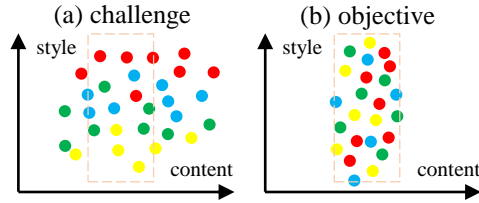


Figure 2: (a) Feature domain for urban-scenes, where the content is similar while the styles have clear gaps; (b) The goal is robust style handling and stable content representing.

3.2 Content-enhanced Mask Attention

Our proposed idea is to enhance the focus of the mask attention mechanism [5, 6] on content information from urban scenes. This enhancement aids the segmentation masks in concentrating on scene content while reducing sensitivity to style variations. Since content/style information is usually more pronounced in the low/high resolution features of an image, it is intuitive to amplify the influence of low-resolution features in the self-attention learning.

Mask Attention Mechanism learns the query features as the segmentation masks by introducing a mask attention matrix based on the self-attention mechanism. Let $\mathbf{F}_l \in \mathbb{R}^{(W_l \cdot H_l) \times C_F}$ denote the image features from the image decoder with a spatial width and height of W_l and H_l , and let $\mathbf{X}_l \in \mathbb{R}^{N \times C}$ denote the features of the l^{th} layer in a Transformer decoder, where N is the number of semantic categories. Further, C_F and C denote the channel dimensions of the image features and self-attention embeddings respectively. \mathbf{X}_0 refers to the input query features of the Transformer decoder. The key $\mathbf{K}_l \in \mathbb{R}^{(W_l \cdot H_l) \times C}$, value $\mathbf{V}_l \in \mathbb{R}^{(W_l \cdot H_l) \times C}$, and query $\mathbf{Q}_l \in \mathbb{R}^{N \times C}$ is computed

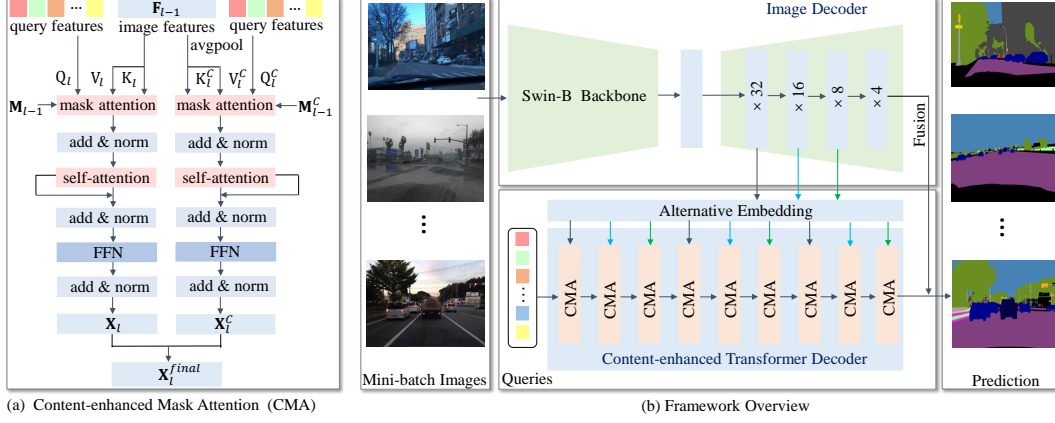


Figure 3: (a) The proposed Content-enhanced Mask Attention (CMA). Apart from the conventional mask attention (left branch), the down-sampled feature maps, which contain more abundant content information, are used to learn content enhanced query features (right branch). (b) Framework overview of the proposed Content-enhanced Mask TransFormer (CMFormer) for domain generalized semantic segmentation. The image decoder is directly inherited from the Mask2Former [6].

by linear transformations f_K , f_V and f_Q , respectively, given by

$$\mathbf{K}_l = f_K(\mathbf{F}_{l-1}), \mathbf{V}_l = f_V(\mathbf{F}_{l-1}), \mathbf{Q}_l = f_Q(\mathbf{X}_{l-1}). \quad (2)$$

Then, the query feature \mathbf{X}_l is computed by

$$\mathbf{X}_l = \text{softmax}(\mathcal{M}_{l-1} + \mathbf{Q}_l \mathbf{K}_l^T) \mathbf{V}_l + \mathbf{X}_{l-1}, \quad (3)$$

where $\mathcal{M}_{l-1} \in \{0, 1\}^{N \times H_l \times W_l}$ is a binary mask attention matrix from the resized mask prediction of the previous $(l-1)^{th}$ layer, with a threshold of 0.5. \mathcal{M}_0 is binarized and resized from \mathbf{X}_0 . It filters the foreground regions of an image, given by

$$\mathcal{M}_{l-1}(x, y) = \begin{cases} 0 & \text{if } \mathcal{M}_{l-1}(x, y) = 1 \\ -\infty & \text{else} \end{cases}. \quad (4)$$

Content Enhancement is incorporated into the mask attention mechanism by acquiring supplementary query features from low-resolution image features. This is based on the understanding that content information tends to be more discriminative, while style information is less sensitive in low-resolution image features. To this end, a parallel branch that leverages low-resolution image features is introduced in each Transformer decoder layer (in Fig. 3a). The content-enhanced image feature $\mathbf{F}_l^c \in \mathbb{R}^{(W_l \cdot H_l) \times C_F}$ is computed by average pooling avgpool from the original image feature $\mathbf{F}_l \in \mathbb{R}^{(W_l \cdot H_l) \times C_F}$ by

$$\mathbf{F}_l^c = \text{avgpool}(\mathbf{F}_l). \quad (5)$$

Following Eq. 2, for the l^{th} Transformer decoder, the content enhanced key $\mathbf{K}_l^c \in \mathbb{R}^{(W_l/2 \cdot H_l/2) \times C}$ and value $\mathbf{V}_l^c \in \mathbb{R}^{(W_l/2 \cdot H_l/2) \times C}$ are computed from the linear transformation of the down-sampled image feature \mathbf{F}_l^c . Then, similar to Eq. 3, the content-enhanced query feature \mathbf{X}_l^c is computed as

$$\mathbf{X}_l^c = \text{softmax}(\mathcal{M}_{l-1}^c + \mathbf{Q}_l \mathbf{K}_l^{cT}) \mathbf{V}_l^c + \mathbf{X}_{l-1}^c, \quad (6)$$

where $\mathcal{M}_{l-1}^c \in \{0, 1\}^{N \times (H_l/2 \cdot W_l/2)}$ also follows the computation of \mathcal{M}_{l-1} defined in Eq. 4.

Content-aware Query Feature Fusion is proposed to merge the query \mathbf{X}_l with content-enhanced query features \mathbf{X}_l^c , allowing for the highlighting of content while retaining the necessary details for semantic prediction. The fused feature \mathbf{X}_l^{final} serves as the final output of the l^{th} Transformer decoder, and it is computed as follows:

$$\mathbf{X}_l^{final} = h_l([\mathbf{X}_l, \mathbf{X}_l^c]), \quad (7)$$

Here, $[\cdot, \cdot]$ represents the concatenation operation, and $h_l(\cdot)$ refers to a linear layer.

3.3 Content-enhancement for Multi-resolution Features

In the process of decoding domain-generalized segmentation predictions from coarse-to-fine image features, it is crucial to enhance the content information at each resolution. This ensures that the

content remains highlighted in the query features of masks, allowing for the learning of segmentation masks that are less sensitive to style variations.

Multi-resolution Features include $\times 32$, $\times 16$ and $\times 8$ resolution features from the image decoder, denoted as $\mathbf{F}^{\times 32}$, $\mathbf{F}^{\times 16}$ and $\mathbf{F}^{\times 8}$, respectively. Following Eq. 2, 3, the key, value and query for $\mathbf{F}^{\times 32}$ and $\mathbf{F}^{\times 16}$ and $\mathbf{F}^{\times 8}$ are denoted by $\mathbf{K}^{\times 32}$, $\mathbf{V}^{\times 32}$, $\mathbf{Q}^{\times 32}$ and $\mathbf{K}^{\times 16}$, $\mathbf{V}^{\times 16}$, $\mathbf{Q}^{\times 16}$ and $\mathbf{K}^{\times 8}$, $\mathbf{V}^{\times 8}$, $\mathbf{Q}^{\times 8}$, respectively.

Content-enhanced Multi-resolution Features are down-sampled from $\times 32$, $\times 16$ and $\times 8$ resolution features $\mathbf{F}^{\times 32}$ and $\mathbf{F}^{\times 16}$ and $\mathbf{F}^{\times 8}$ into $\mathbf{F}^{\times 32,c}$ and $\mathbf{F}^{\times 16,c}$ and $\mathbf{F}^{\times 8,c}$ by following Eq. 5. Also following Eq. 2, 3, the key, value and query for $\mathbf{F}^{\times 32,c}$ and $\mathbf{F}^{\times 16,c}$ and $\mathbf{F}^{\times 8,c}$ are denoted as $\mathbf{K}^{\times 32,c}$, $\mathbf{V}^{\times 32,c}$, $\mathbf{Q}^{\times 32,c}$ and $\mathbf{K}^{\times 16,c}$, $\mathbf{V}^{\times 16,c}$, $\mathbf{Q}^{\times 16,c}$ and $\mathbf{K}^{\times 8,c}$, $\mathbf{V}^{\times 8,c}$, $\mathbf{Q}^{\times 8,c}$, respectively.

Multi-resolution Feature Fusion to the Transformer Decoder directly follows the original Mask2Former [6], which alternatively learns the image features from each different resolution. As there are 9 self-attention layers in the Transformer decoder, the first, fourth, seventh layers take the $\times 32$ image features as input (**black** down-arrows in Fig. 3b), the second, fifth, eighth layers take the $\times 16$ image features as the input (**blue** downarrows in Fig. 3b), and the third, sixth, ninth layer take the $\times 8$ image features as the input (**green** downarrows in Fig. 3b).

Taking the first, fourth, seventh layers with $\times 32$ image features as an example (here $l = 1, 4, 7$), the content-enhanced learning process is given by

$$\mathbf{X}_l = \text{softmax}(\mathcal{M}_{l-1} + \mathbf{Q}_l^{\times 32} \mathbf{K}_l^{\times 32T}) \mathbf{V}_l^{\times 32} + \mathbf{X}_{l-1}^{final}, \quad (8)$$

$$\mathbf{X}_l^c = \text{softmax}(\mathcal{M}_{l-1}^c + \mathbf{Q}_{l-1}^{\times 32,c} \mathbf{K}^{\times 32,cT}) \mathbf{V}^{\times 32,c} + \mathbf{X}_{l-1}^{final}, \quad (9)$$

Following Eq. 7, \mathbf{X}_l^c and \mathbf{X}_l are merged to compute the final output of this decoder layer, denoted as \mathbf{X}_l^{final} . For the first layer, \mathbf{X}_0^{final} is equivalent to \mathbf{X}_0 , which is the input query features of the Transformer decoder.

The content enhance learning of the second, fifth and eighth layer follows Eq. 8, 9 but uses the $\mathbf{K}^{\times 16,c}$, $\mathbf{V}^{\times 16,c}$, $\mathbf{Q}^{\times 16,c}$ and $\mathbf{K}^{\times 16}$, $\mathbf{V}^{\times 16}$, $\mathbf{Q}^{\times 16}$ as input. The third, sixth and ninth layer also follow Eq. 8, 9 but takes $\mathbf{K}^{\times 8,c}$, $\mathbf{V}^{\times 8,c}$, $\mathbf{Q}^{\times 8,c}$ and $\mathbf{K}^{\times 8}$, $\mathbf{V}^{\times 8}$, $\mathbf{Q}^{\times 8}$ as input.

3.4 Network Architecture and Implementation Details

The overall framework is shown in Fig. 3b. The Swin-Base Transformer [27] is used as the backbone, and the image decoder is inherited from Mask2Former [6]. The pre-trained model from ImageNet [9] is utilized for initialization.

The image decoder from [6] uses the off-the-shelf multi-scale deformable attention Transformer (MSDeformAttn) [68] with the default setting in [68, 6]. By considering the image features from the Swin-Based encoder as input, every 6 MSDeformAttn layers are used to progressively up-sample the image features in $\times 32$, $\times 16$, $\times 8$, and $\times 4$, respectively. The $1/4$ resolution feature map is fused with the features from the Transformer decoder for dense prediction.

Following the default setting of MaskFormer [5] and Mask2Former [6], the final loss function \mathcal{L} is a linear combination of the binary cross-entropy loss \mathcal{L}_{ce} , dice loss \mathcal{L}_{dice} , and the classification loss \mathcal{L}_{cls} , given by

$$\mathcal{L} = \lambda_{ce} \mathcal{L}_{ce} + \lambda_{dice} \mathcal{L}_{dice} + \lambda_{cls} \mathcal{L}_{cls}, \quad (10)$$

with hyper-parameters $\lambda_{ce} = \lambda_{dice} = 5.0$, $\lambda_{cls} = 2.0$ as the default of Mask2Former without any tuning. The Adam optimizer is used with an initial learning rate of 1×10^{-4} . The weight decay is set 0.05. The training terminates after 50 epochs.

4 Experiment

4.1 Dataset & Evaluation Protocols

Building upon prior research in domain-generalized USSS, our experiments utilize five different semantic segmentation datasets. Specifically, CityScapes [8] provides 2,975 and 500 well-annotated samples for training and validation, respectively. These driving-scenes are captured in Germany cities with a resolution of 2048×1024 . BDD-100K [59] also provides diverse urban driving scenes with a resolution of 1280×720 . 7,000 and 1,000 fine-annotated samples are provided for training and validation of semantic segmentation, respectively. Mapillary [33] is also a real-scene large-scale semantic segmentation dataset with 25,000 samples. SYNTHIA [43] is large-scale synthetic dataset,

Table 1: Performance comparison of the proposed CMFormer compared to existing domain generalized USSS methods. The symbol ‘-’ indicates cases where the metric is either not reported or the official source code is not available. Evaluation metric mIoU is given in (%).

Method	Proc. & Year	Trained on GTA5 (G)				Trained on SYNTHIA (S)				Trained on Cityscapes (C)			
		→ C	→ B	→ M	→ S	→ C	→ B	→ M	→ G	→ B	→ M	→ G	→ S
IBN [35]	ECCV2018	33.85	32.30	37.75	27.90	32.04	30.57	32.16	26.90	48.56	57.04	45.06	26.14
IW [36]	CVPR2019	29.91	27.48	29.71	27.61	28.16	27.12	26.31	26.51	48.49	55.82	44.87	26.10
Itemnorm [17]	CVPR2019	31.81	32.70	33.88	27.07	-	-	-	-	49.23	56.26	45.73	25.98
DRPC [62]	ICCV2019	37.42	32.14	34.12	28.06	35.65	31.53	32.74	28.75	49.86	56.34	45.62	26.58
ISW [7]	CVPR2021	36.58	35.20	40.33	28.30	35.83	31.62	30.84	27.68	50.73	58.64	45.00	26.20
GTR [37]	TIP2021	37.53	33.75	34.52	28.17	36.84	32.02	32.89	28.02	50.75	57.16	45.79	26.47
DRL [57]	AAAI2022	41.04	39.15	41.60	-	-	-	-	-	51.80	-	46.52	26.50
SHADE [65]	ECCV2022	44.65	39.28	43.34	-	-	-	-	-	50.95	60.67	48.61	27.62
SAW [38]	CVPR2022	39.75	37.34	41.86	30.79	38.92	35.24	34.52	29.16	52.95	59.81	47.28	28.32
WildNet [23]	CVPR2022	44.62	38.42	46.09	31.34	-	-	-	-	50.94	58.79	47.01	27.95
AdvStyle [66]	NeurIPS2022	39.62	35.54	37.00	-	37.59	27.45	31.76	-	-	-	-	-
CMFormer (Ours)	2023	55.31	49.91	60.09	43.80	44.59	33.44	43.25	40.65	59.27	71.10	58.11	40.43
		↑10.66	↑10.63	↑14.00	↑12.46	↑5.67	↓1.80	↑8.73	↑11.49	↑6.32	↑10.43	↑9.50	↑12.11

and provides 9,400 images with a resolution of 1280×760. GTA5 [42] is a synthetic semantic segmentation dataset rendered by the GTAV game engine. It provides 24,966 simulated urban-street samples with a resolution of 1914×1052. We use C, B, M, S and G to denote these five datasets.

Following prior domain generalized USSS works [35, 36, 7, 38], the segmentation model is trained on one dataset as the source domain, and is validated on the rest of the four datasets as the target domains. Three settings include: 1) G to C, B, M, S; 2) S to C, B, M, G; and 3) C to B, M, G, S. mIoU (in percentage %) is used as the validation metric. All of our experiments are performed three times and averaged for fair comparison. All the reported performance is directly cited from prior works under the ResNet-50 backbone [35, 36, 7, 38].

4.2 Comparison with State-of-the-art Domain Generalized USSS Methods

GTA5 Source Domain The third column of Table 1 reports the performance on target domains of C, B, M and S, respectively. The proposed CMFormer shows a performance improvement of 10.66%, 10.63%, 14.00% and 12.46% compared to existing state-of-the-art CNN based methods on each target domain, respectively. These outcomes demonstrate the feature generalization ability of the proposed CMFormer. Notice that the source domain GTA5 is a synthetic dataset, while the target domains are real images. It further validates the performance of the proposed method.

SYNTHIA Source Domain The forth column of Table 1 reports the performance. The proposed CMFormer shows a 5.67%, 8.73% and 11.49% mIoU performance gain against the best CNN based methods, respectively. However, on the BDD-100K (B) dataset, the semantic-aware whitening (SAW) method [38] outperforms the proposed CMFormer by 1.80% mIoU. Nevertheless, the proposed CMFormer still outperforms the rest state-of-the-art methods. The performance gain of the proposed CMFormer when trained on SYNTHIA dataset is not as significant as it is trained on CityScapes or GTA5 dataset. The explanation may be that the SYNTHIA dataset has much fewer samples than GTA5 dataset, *i.e.*, 9400 v.s. 24966, and a transformer may be under-trained.

CityScapes Source Domain The last column of Table 1 reports the performance. The proposed CMFormer shows a performance gain of 6.32%, 10.43%, 9.50% and 12.11% mIoU on the B, M, G and S dataset against the state-of-the-art CNN based method. As BDD100K dataset contains many high-time urban-street images, it is particularly challenging for existing domain generalized USSS methods. Still, a performance gain of 6.32% is observed by the proposed CMFormer.

4.3 Ablation Studies

On Content-enhancement of Each Resolution Table 2 reports the performance of the proposed CMFormer when ×32, ×16 and ×8 image features are implemented with content enhancement. When no image features are implemented with content enhancement, CMFormer degrades into a Mask2Former [6] with Swin-Base backbone. When only implementing content enhancement on the ×32 image feature, the down-sampled ×128 image feature may propagate little content information to the segmentation mask, and only a performance gain of 0.74%, 1.43%, 0.37% and 0.64% on B, M, G and S target domain is observed. When further implementing content enhancement on the ×16 image feature, the enhanced content information begins to play a role, and an additional performance gain of 1.93%, 2.17%, 0.12% and 0.58% is observed. Then, the content enhancement on the ×8

Table 2: Ablation studies on each component of the proposed CMFormer. $\times 32$, $\times 16$ and $\times 8$ denote the image features of $\times 32$, $\times 16$ and $\times 8$ resolution. \checkmark refers to the content enhancement is implemented. Evaluation metric mIoU is presented in (%).

Content Enhancement			Trained on CityScapes (C)				Trained on SYNTHIA (S)			
$\times 32$	$\times 16$	$\times 8$	$\rightarrow B$	$\rightarrow M$	$\rightarrow G$	$\rightarrow S$	$\rightarrow C$	$\rightarrow B$	$\rightarrow M$	$\rightarrow G$
			55.43	66.12	55.05	38.19	42.64	31.91	36.80	37.29
\checkmark			56.17	67.55	55.42	38.83	42.77	31.62	41.61	37.56
\checkmark	\checkmark		58.10	69.72	55.54	39.41	44.22	33.19	42.23	38.78
\checkmark	\checkmark	\checkmark	59.27	71.10	58.11	40.43	44.59	33.44	43.25	40.65

Table 3: Ablation studies on the embedding order of the multi-resolution features in the CMFormer. Ours are compared with the plain and descent settings. Evaluation metric mIoU in %.

Method	Trained on Cityscapes (C)			
	$\rightarrow B$	$\rightarrow M$	$\rightarrow G$	$\rightarrow S$
<i>plain</i>	59.20	71.08	57.89	40.16
<i>descent</i>	58.51	71.01	57.53	40.29
Ours	59.27	71.10	58.11	40.43

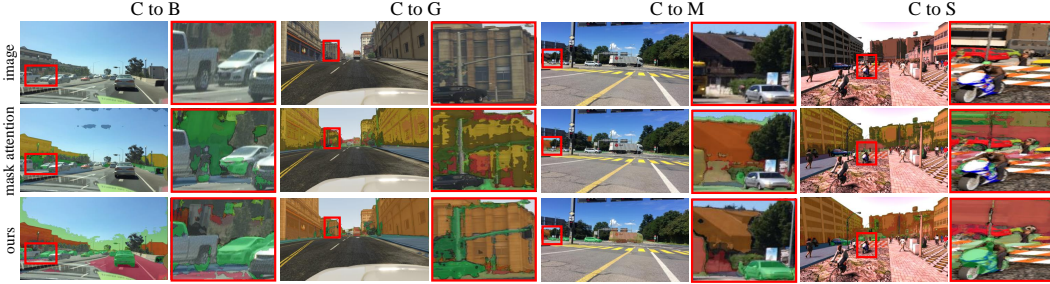


Figure 4: Visualization of the segmentation masks learnt by the original mask attention (in second row) and the proposed content-enhanced mask attention (in third row), under the C [8] \rightarrow B [59], G [42], M [33], S [43] settings (in first row). The proposed content-enhanced mask attention is less sensitive to the style variation and is of better capability to separate the objects from background.

image feature also demonstrates a significant impact on the generalization ability. Similar observation can be found on the S \rightarrow C, B, M, G setting.

To better understand the content enhancement for mask attention, some segmentation masks learnt by the existing mask attention and our content enhanced mask attention are visualized in the second and third row of Fig. 4. The proposed content enhanced mask attention is less sensitive to the style variation. The learnt masks are more capable to separate the key objects from the background.

On Multi-resolution Feature Embedding Strategy is inherited from Mask2Former in an alternative manner [6]. To investigate its effectiveness, the method is compared with two alternative solutions: (1) plain sequence embedding (denoted as *plain*) and (2) alternative embedding in a descent order (denoted as *descent*). For the plain sequence embedding, the first, second and third three decoder layers are fed into the $\times 32$, $\times 16$ and $\times 8$ image features, respectively. For the alternative embedding in a descent order, each three decoder layers are fed into the image features with the order of $\times 8$, $\times 16$ and $\times 32$. The results are listed in Table 3. The embedding strategy inherited from [6] has a slightly better performance compared to the two other solutions.

4.4 Comparison with Recent State-of-the-art in Related Tasks

The proposed CMFormer is compared against three categories of recent state-of-the-art approaches that are relevant to related tasks. While these approaches do not specifically focus on domain-generalized USSS, we compare them to further highlight the optimality of the proposed CMFormer.

Specially, we consider mask-level Transformer segmentation models (Segmenter [47], MaskFormer [5], Mask2Former [6], denoted as \mathcal{M}), combining state-of-the-art CNN based domain generalization techniques with segmentation Transformer (denoted as \mathcal{G}), and the plain segmentation Transformer that is pre-trained from the foundation models (SAM [21], SegGPT [54], denoted as \mathcal{F}). It can be seen that the proposed CMFormer significantly outperforms other methods. It is also very interesting to observe that the whitening transformation (IW [36], ISW [36], SAW [38]) for CNN based domain generalized segmentation frameworks do not work for mask-level Transformer segmentation pipeline.

4.5 Extra Experiments on Generalization

To Adverse Domains Beyond the standard validation protocols in existing methods [35, 16, 36, 7, 38, 66], we further validate the proposed CMFormer’s performance by benchmarking it on the

Table 4: Performance comparison of the proposed CMFormer against the state-of-the-art mask Transformer models for semantic segmentation (denoted as \mathcal{M}), state-of-the-art domain generalization approaches (denoted as \mathcal{G}), and plain Transformer models pre-trained on foundational models (denoted as \mathcal{F}). Evaluation metric mIoU is presented in (%).

Method	Backbone	Category	Trained on Cityscapes (C)			
			\rightarrow B	\rightarrow M	\rightarrow G	\rightarrow S
Segmenter [47]	ViT-B	\mathcal{M}	31.42	37.76	28.56	17.32
Max-DeepLab [51]	MaX-L		47.82	54.05	39.82	27.15
CMT-DeepLab [60]	Axial-R104		48.74	57.93	41.66	26.06
kMaX-DeepLab [61]	ConvNeXt-B		50.58	59.06	43.92	28.70
MaskFormer [5]	Swin-B		51.86	64.70	49.24	33.35
Mask2Former [6]	Swin-B		55.43	66.12	55.05	38.19
IN [35] + Mask2Former [6]	Swin-B	\mathcal{G}	56.78	67.97	56.07	40.16
IW [36] + Mask2Former [6]	Swin-B		54.20	63.14	50.57	35.59
ISW [36] + Mask2Former [6]	Swin-B		53.00	63.16	52.14	36.97
SAW [38] + Mask2Former [6]	Swin-B		55.78	62.36	57.88	39.96
SAM Pre-trained [21]	ViT-H	\mathcal{F}	52.36	65.72	51.49	34.25
SegGPT Pre-trained [54]	ViT-L		50.94	61.37	44.85	32.36
CMFormer (Ours)	Swin-B	\mathcal{G}	59.27	71.10	58.11	40.43

Table 5: Generalization of the proposed CMFormer to the adverse condition domains (rain, fog, night and snow) on ACDC dataset [44]. Evaluation metric mIoU is in %.

Method	Backbone	Trained on Cityscapes (C)				
		\rightarrow Fog	\rightarrow Night	\rightarrow Rain	\rightarrow Snow	mean
IN [35]	ResNet-50	63.8	21.2	50.4	49.6	43.7
Iternorm [16]	ResNet-50	63.3	23.8	50.1	49.9	45.3
IW [36]	ResNet-50	62.4	21.8	52.4	47.6	46.6
ISW [7]	ResNet-50	64.3	24.3	56.0	49.8	48.1
ISSA [25]	MiT-B2	67.5	33.2	55.9	53.2	52.5
RefineNet [26]	ResNet-101	46.4	29.0	52.6	43.3	43.7
DeepLabv3+ [3]	ResNet-101	45.7	25.0	50.0	42.0	41.6
DANet [12]	ResNet-101	34.7	19.1	41.5	33.3	33.1
HRNet [52]	HR-w48	38.4	20.6	44.8	35.1	35.3
SegFormer [56]	MiT-B2	59.2	38.9	62.5	58.2	56.2
Mask2Former [6]	Swin-B	73.4	37.1	63.6	62.5	58.0
CMFormer (Ours)	Swin-B	77.8	33.7	67.6	64.3	60.1

adverse conditions dataset with correspondance (ACDC) [44]. It is the largest semantic segmentation dataset under a variety of adverse conditions, including rain, fog, night and snow. We set the fog, night, rain and snow as four different unseen domains, and directly use the model pre-trained on CityScapes for inference. The results are shown in Table 5. It significantly outperforms existing domain generalized segmentation methods (IN [35], Iternorm [16], IW [36], ISW [7], ISSA [25]) by upto 10.3%, 0.5%, 11.6%, 11.1% on the fog, night, rain and snow domains, respectively. On the other hand, it shows a superior performance of 4.4%, 4.0% and 1.8% against the second best-performed method Mask2Former on the fog, rain and snow domain, respectively.

From Synthetic Domain to Real Domain We also test the generalization ability of the CMFormer when trained on the synthetic domains (G+S) and validated on the three real-world domains B, C and M, respectively. The results are shown in Table 6. The proposed CMFormer significantly outperforms the instance normalization based (IBN [35]), whitening transformation based (ISW [7]) and adversarial domain training based (SHADE [65], AdvStyle [66]) methods by $>10\%$ mIoU.

4.6 Visualization

T-SNE visualization To better understand the style change handling and stable robust representation learning, the feature space with samples when using B, M, G, S as target domains are shown in Fig. 5 by t-SNE. ISW [7], a typical style-decoupling method, has some difficulty to handle the style variation, but the distance of the semantic embeddings from each domain is close. Advstyle [66], a typical adverse style augmentation method, can better mix the styles, but the distance of semantic embeddings is not properly reduced. The original mask attention from [6] can reduce the distance of each semantic embedding but still has some difficulty to mix the different styles. In contrast, the proposed CMFormer can not only reduce the distance of semantic embeddings, but also allow the styles to be more uniformly distributed and therefore minimizes the domain gap.

Quantitative segmentation prediction Some generalized segmentation prediction results on the $C \rightarrow B, M, G, S$ setting (in Fig. 9) and on the $C \rightarrow$ adverse domain setting (in Fig. 10). Compared with the CNN based methods, the proposed CMFormer shows a better segmentation prediction, especially in terms of the completeness of objects.

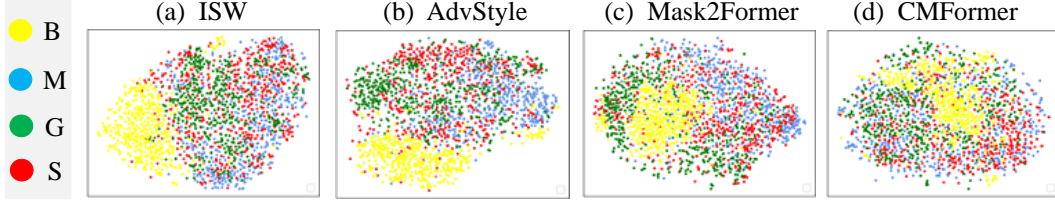


Figure 5: T-SNE visualization of the features space on target domains. (a) ISW [7], (b) AdvStyle [66], (c) Mask2Former [6], (d) the proposed CMFormer. Our method has the most uniform distribution, which means the domain gap is minimized.

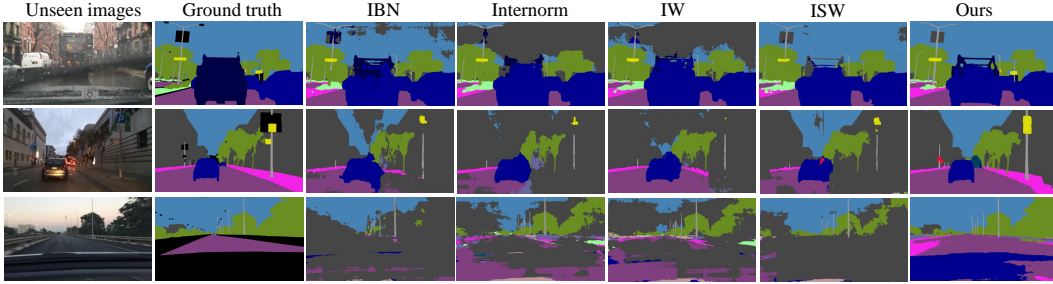


Figure 6: Unseen domain segmentation prediction of existing CNN based domain generalized semantic segmentation methods (IBN [35], IW [36], Iternorm [17], ISW [7]) and the proposed CMFormer under the $C \rightarrow B$ setting. More segmentation prediction is in the supplementary material.

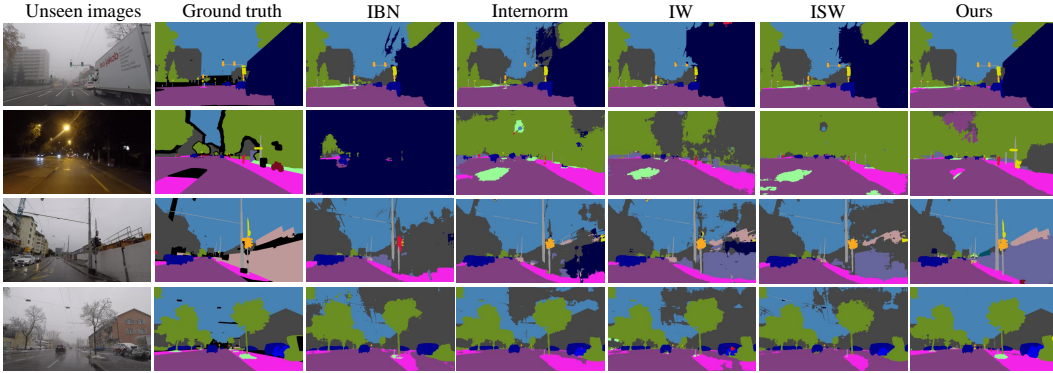


Figure 7: Unseen domain segmentation prediction of existing CNN based domain generalized semantic segmentation methods (IBN [35], IW [36], Iternorm [17], ISW [7]) and the proposed CMFormer under the $C \rightarrow$ adverse domain setting. More prediction is in the supplementary material.

5 Conclusion

In this paper, we explored the feasibility of adapting the mask Transformer for domain-generalized urban-scene semantic segmentation (USSS). To address the challenges of style variation and robust content representation, we proposed a content-enhanced mask attention mechanism. This mechanism is designed to capture more resilient content features while being less sensitive to style variations. Furthermore, we extended it to incorporate multi-resolution features and integrate it into a novel framework called the **Content-enhanced Mask TransFormer** (CMFormer). To evaluate the effectiveness of CMFormer, we conducted extensive experiments on multiple settings. The results demonstrated the superior performance of CMFormer compared to existing domain-generalized USSS methods.

Limitation Discussion & Boarder Social Impact. The proposed content-enhanced mask attention mechanism is derived from the self-attention mechanism and can be seamlessly integrated into ViT based segmentation pipelines. The experimental results demonstrate its superior performance, thereby indicating the potential to shift the focus of domain-generalized USSS towards ViT based pipelines.

Given the criticality of safety-related road applications, the proposed method holds significant importance. It has the potential to enhance the accuracy and reliability of semantic segmentation models, thereby contributing to safer and more efficient autonomous systems. Overall, the proposed content-enhanced mask attention mechanism not only offers promising advancements in domain-generalized USSS but also holds potential for broader applications in real-world scenarios.

References

- [1] Fabio M Carlucci, Antonio D’Innocente, Silvia Bucci, Barbara Caputo, and Tatiana Tommasi. Domain generalization by solving jigsaw puzzles. In *Proceedings of the IEEE/CVF Conference on Computer Vision and Pattern Recognition*, pages 2229–2238, 2019.
- [2] Prithvijit Chattopadhyay, Yogesh Balaji, and Judy Hoffman. Learning to balance specificity and invariance for in and out of domain generalization. In *European Conference on Computer Vision*, pages 301–318. Springer, 2020.
- [3] Liang-Chieh Chen, Yukun Zhu, George Papandreou, Florian Schroff, and Hartwig Adam. Encoder-decoder with atrous separable convolution for semantic image segmentation. In *Proceedings of the European conference on computer vision (ECCV)*, pages 801–818, 2018.
- [4] Wei-Ting Chen, Zhi-Kai Huang, Cheng-Che Tsai, Hao-Hsiang Yang, Jian-Jiun Ding, and Sy-Yen Kuo. Learning multiple adverse weather removal via two-stage knowledge learning and multi-contrastive regularization: Toward a unified model. In *Proceedings of the IEEE/CVF Conference on Computer Vision and Pattern Recognition (CVPR)*, pages 17653–17662, 2022.
- [5] Bowen Cheng, Alex Schwing, and Alexander Kirillov. Per-pixel classification is not all you need for semantic segmentation. *Advances in Neural Information Processing Systems*, 34:17864–17875, 2021.
- [6] Bowen Cheng, Ishan Misra, Alexander G Schwing, Alexander Kirillov, and Rohit Girdhar. Masked-attention mask transformer for universal image segmentation. In *Proceedings of the IEEE/CVF Conference on Computer Vision and Pattern Recognition (CVPR)*, pages 1290–1299, 2022.
- [7] S. Choi, S. Jung, H. Yun, J. Kim, S. Kim, and J. Choo. Robustnet: Improving domain generalization in urban-scene segmentation via instance selective whitening. In *Proceedings of the IEEE/CVF Conference on Computer Vision and Pattern Recognition (CVPR)*, pages 11580–11590, 2021.
- [8] Marius Cordts, Mohamed Omran, Sebastian Ramos, Timo Rehfeld, Markus Enzweiler, Rodrigo Benenson, Uwe Franke, Stefan Roth, and Bernt Schiele. The cityscapes dataset for semantic urban scene understanding. In *Proceedings of the IEEE conference on computer vision and pattern recognition*, pages 3213–3223, 2016.
- [9] Jia Deng, Wei Dong, Richard Socher, Li-Jia Li, Kai Li, and Li Fei-Fei. Imagenet: A large-scale hierarchical image database. In *2009 IEEE conference on computer vision and pattern recognition*, pages 248–255. Ieee, 2009.
- [10] Carlos A Diaz-Ruiz, Youya Xia, Yurong You, Jose Nino, Junan Chen, Josephine Monica, Xiangyu Chen, Katie Luo, Yan Wang, Marc Emond, et al. Ithaca365: Dataset and driving perception under repeated and challenging weather conditions. In *Proceedings of the IEEE/CVF Conference on Computer Vision and Pattern Recognition (CVPR)*, pages 21383–21392, 2022.
- [11] Alexey Dosovitskiy, Lucas Beyer, Alexander Kolesnikov, Dirk Weissenborn, Xiaohua Zhai, Thomas Unterthiner, Mostafa Dehghani, Matthias Minderer, Georg Heigold, Sylvain Gelly, et al. An image is worth 16x16 words: Transformers for image recognition at scale. In *International Conference on Learning Representations*, 2020.
- [12] Jun Fu, Jing Liu, Haijie Tian, Yong Li, Yongjun Bao, Zhiwei Fang, and Hanqing Lu. Dual attention network for scene segmentation. In *Proceedings of the IEEE/CVF conference on computer vision and pattern recognition*, pages 3146–3154, 2019.
- [13] Sivan Harary, Eli Schwartz, Assaf Arbelle, Peter Staar, Shady Abu-Hussein, Elad Amrani, Roei Herzig, Amit Alfassy, Raja Giryes, Hilde Kuehne, et al. Unsupervised domain generalization by learning a bridge across domains. In *Proceedings of the IEEE/CVF Conference on Computer Vision and Pattern Recognition*, pages 5280–5290, 2022.
- [14] Kaiming He, Xiangyu Zhang, Shaoqing Ren, and Jian Sun. Deep residual learning for image recognition. In *Proceedings of the IEEE conference on computer vision and pattern recognition*, pages 770–778, 2016.
- [15] Conghui Hu and Gim Hee Lee. Feature representation learning for unsupervised cross-domain image retrieval. In *European Conference on Computer Vision*, pages 529–544. Springer, 2022.
- [16] L. Huang, Y. Zhou, F. Zhu, L. Liu, and L. Shao. Iterative normalization: Beyond standardization towards efficient whitening. In *Proceedings of the IEEE/CVF Conference on Computer Vision and Pattern Recognition (CVPR)*, pages 4874–4883, 2019.

- [17] Lei Huang, Yi Zhou, Fan Zhu, Li Liu, and Ling Shao. Iterative normalization: Beyond standardization towards efficient whitening. In *Proceedings of the IEEE/CVF conference on computer vision and pattern recognition*, pages 4874–4883, 2019.
- [18] Zeyi Huang, Haohan Wang, Eric P Xing, and Dong Huang. Self-challenging improves cross-domain generalization. In *Computer Vision—ECCV 2020: 16th European Conference, Glasgow, UK, August 23–28, 2020, Proceedings, Part II 16*, pages 124–140. Springer, 2020.
- [19] Wei Ji, Shuang Yu, Junde Wu, Kai Ma, Cheng Bian, Qi Bi, Jingjing Li, Hanruo Liu, Li Cheng, and Yefeng Zheng. Learning calibrated medical image segmentation via multi-rater agreement modeling. In *Proceedings of the IEEE/CVF Conference on Computer Vision and Pattern Recognition*, pages 12341–12351, 2021.
- [20] Jin Kim, Jiyoung Lee, Jungin Park, Dongbo Min, and Kwanghoon Sohn. Pin the memory: Learning to generalize semantic segmentation. In *Proceedings of the IEEE/CVF Conference on Computer Vision and Pattern Recognition*, pages 4350–4360, 2022.
- [21] Alexander Kirillov, Eric Mintun, Nikhila Ravi, Hanzi Mao, Chloe Rolland, Laura Gustafson, Tete Xiao, Spencer Whitehead, Alexander C Berg, Wan-Yen Lo, et al. Segment anything. *arXiv preprint arXiv:2304.02643*, 2023.
- [22] John Lambert, Zhuang Liu, Ozan Sener, James Hays, and Vladlen Koltun. Mseg: A composite dataset for multi-domain semantic segmentation. In *Proceedings of the IEEE/CVF conference on computer vision and pattern recognition*, pages 2879–2888, 2020.
- [23] Suhyeon Lee, Hongje Seong, Seongwon Lee, and Euntai Kim. Wildnet: Learning domain generalized semantic segmentation from the wild. In *Proceedings of the IEEE/CVF Conference on Computer Vision and Pattern Recognition*, pages 9936–9946, 2022.
- [24] Mike Li, Hongseok Namkoong, and Shangzhou Xia. Evaluating model performance under worst-case subpopulations. *Advances in Neural Information Processing Systems*, 34:17325–17334, 2021.
- [25] Yumeng Li, Dan Zhang, Margret Keuper, and Anna Khoreva. Intra-source style augmentation for improved domain generalization. In *Proceedings of the IEEE/CVF Winter Conference on Applications of Computer Vision*, pages 509–519, 2023.
- [26] Guosheng Lin, Anton Milan, Chunhua Shen, and Ian Reid. Refinenet: Multi-path refinement networks for high-resolution semantic segmentation. In *Proceedings of the IEEE conference on computer vision and pattern recognition*, pages 1925–1934, 2017.
- [27] Ze Liu, Yutong Lin, Yue Cao, Han Hu, Yixuan Wei, Zheng Zhang, Stephen Lin, and Baining Guo. Swin transformer: Hierarchical vision transformer using shifted windows. In *Proceedings of the IEEE/CVF International Conference on Computer Vision (CVPR)*, pages 10012–10022, 2021.
- [28] Ze Liu, Han Hu, Yutong Lin, Zhuliang Yao, Zhenda Xie, Yixuan Wei, Jia Ning, Yue Cao, Zheng Zhang, Li Dong, et al. Swin transformer v2: Scaling up capacity and resolution. In *Proceedings of the IEEE/CVF Conference on Computer Vision and Pattern Recognition (CVPR)*, pages 12009–12019, 2022.
- [29] Divyat Mahajan, Shruti Tople, and Amit Sharma. Domain generalization using causal matching. In *International Conference on Machine Learning*, pages 7313–7324. PMLR, 2021.
- [30] Toshihiko Matsuura and Tatsuya Harada. Domain generalization using a mixture of multiple latent domains. In *Proceedings of the AAAI Conference on Artificial Intelligence*, volume 34, pages 11749–11756, 2020.
- [31] M Jehanzeb Mirza, Marc Masana, Horst Possegger, and Horst Bischof. An efficient domain-incremental learning approach to drive in all weather conditions. In *Proceedings of the IEEE/CVF Conference on Computer Vision and Pattern Recognition (CVPR)*, pages 3001–3011, 2022.
- [32] Saeid Motiian, Marco Piccirilli, Donald A Adjeroh, and Gianfranco Doretto. Unified deep supervised domain adaptation and generalization. In *Proceedings of the IEEE international conference on computer vision*, pages 5715–5725, 2017.
- [33] Gerhard Neuhold, Tobias Ollmann, Samuel Rota Buló, and Peter Kotschieder. The mapillary vistas dataset for semantic understanding of street scenes. In *Proceedings of the IEEE international conference on computer vision*, pages 4990–4999, 2017.
- [34] Junwen Pan, Qi Bi, Yanzhan Yang, Pengfei Zhu, and Cheng Bian. Label-efficient hybrid-supervised learning for medical image segmentation. In *Proceedings of the AAAI Conference on Artificial Intelligence*, volume 36, pages 2026–2034, 2022.

- [35] X. Pan, P. Luo, J. Shi, and X. Tang. Two at once: Enhancing learning and generalization capacities via ibn-net. In *Proceedings of the European Conference on Computer Vision (ECCV)*, pages 464–479, 2018.
- [36] X. Pan, X. Zhan, J. Shi, X. Tang, and P. Luo. Switchable whitening for deep representation learning. In *Proceedings of the IEEE/CVF Conference on Computer Vision and Pattern Recognition (CVPR)*, pages 1863–1871, 2019.
- [37] Duo Peng, Yinjie Lei, Lingqiao Liu, Pingping Zhang, and Jun Liu. Global and local texture randomization for synthetic-to-real semantic segmentation. *IEEE Transactions on Image Processing*, 30:6594–6608, 2021.
- [38] Duo Peng, Yinjie Lei, Munawar Hayat, Yulan Guo, and Wen Li. Semantic-aware domain generalized segmentation. In *Proceedings of the IEEE/CVF Conference on Computer Vision and Pattern Recognition*, pages 2594–2605, 2022.
- [39] Xi Peng, Fengchun Qiao, and Long Zhao. Out-of-domain generalization from a single source: An uncertainty quantification approach. *IEEE Transactions on Pattern Analysis and Machine Intelligence*, 2022.
- [40] Fabrizio J Piva, Daan de Geus, and Gijs Dubbelman. Empirical generalization study: Unsupervised domain adaptation vs. domain generalization methods for semantic segmentation in the wild. In *Proceedings of the IEEE/CVF Winter Conference on Applications of Computer Vision*, pages 499–508, 2023.
- [41] Fengchun Qiao, Long Zhao, and Xi Peng. Learning to learn single domain generalization. In *Proceedings of the IEEE/CVF Conference on Computer Vision and Pattern Recognition*, pages 12556–12565, 2020.
- [42] Stephan R Richter, Vibhav Vineet, Stefan Roth, and Vladlen Koltun. Playing for data: Ground truth from computer games. In *European conference on computer vision*, pages 102–118. Springer, 2016.
- [43] German Ros, Laura Sellart, Joanna Materzynska, David Vazquez, and Antonio M Lopez. The synthia dataset: A large collection of synthetic images for semantic segmentation of urban scenes. In *Proceedings of the IEEE conference on computer vision and pattern recognition*, pages 3234–3243, 2016.
- [44] Christos Sakaridis, Dengxin Dai, and Luc Van Gool. Acdc: The adverse conditions dataset with correspondences for semantic driving scene understanding. In *Proceedings of the IEEE/CVF International Conference on Computer Vision (ICCV)*, pages 10765–10775, 2021.
- [45] Mattia Segu, Alessio Tonioni, and Federico Tombari. Batch normalization embeddings for deep domain generalization. *Pattern Recognition*, 135:109115, 2023.
- [46] Karen Simonyan and Andrew Zisserman. Very deep convolutional networks for large-scale image recognition. *arXiv preprint arXiv:1409.1556*, 2014.
- [47] Robin Strudel, Ricardo Garcia, Ivan Laptev, and Cordelia Schmid. Segmenter: Transformer for semantic segmentation. In *Proceedings of the IEEE/CVF international conference on computer vision*, pages 7262–7272, 2021.
- [48] Gabriel Tjio, Ping Liu, Joey Tianyi Zhou, and Rick Siow Mong Goh. Adversarial semantic hallucination for domain generalized semantic segmentation. In *Proceedings of the IEEE/CVF Winter Conference on Applications of Computer Vision*, pages 318–327, 2022.
- [49] Vladimir Vapnik. *The nature of statistical learning theory*. Springer science & business media, 2013.
- [50] Riccardo Volpi, Hongseok Namkoong, Ozan Sener, John C Duchi, Vittorio Murino, and Silvio Savarese. Generalizing to unseen domains via adversarial data augmentation. *Advances in neural information processing systems*, 31, 2018.
- [51] Huiyu Wang, Yukun Zhu, Hartwig Adam, Alan Yuille, and Liang-Chieh Chen. Max-deeplab: End-to-end panoptic segmentation with mask transformers. In *Proceedings of the IEEE/CVF conference on computer vision and pattern recognition*, pages 5463–5474, 2021.
- [52] Jingdong Wang, Ke Sun, Tianheng Cheng, Borui Jiang, Chaorui Deng, Yang Zhao, Dong Liu, Yadong Mu, Mingkui Tan, Xinggang Wang, et al. Deep high-resolution representation learning for visual recognition. *IEEE transactions on pattern analysis and machine intelligence*, 43(10):3349–3364, 2020.
- [53] Shujun Wang, Lequan Yu, Caizi Li, Chi-Wing Fu, and Pheng-Ann Heng. Learning from extrinsic and intrinsic supervisions for domain generalization. In *European Conference on Computer Vision*, pages 159–176. Springer, 2020.

- [54] Xinlong Wang, Xiaosong Zhang, Yue Cao, Wen Wang, Chunhua Shen, and Tiejun Huang. Seggpt: Segmenting everything in context. *arXiv preprint arXiv:2304.03284*, 2023.
- [55] Zijian Wang, Yadan Luo, Ruihong Qiu, Zi Huang, and Mahsa Baktashmotlagh. Learning to diversify for single domain generalization. In *Proceedings of the IEEE/CVF International Conference on Computer Vision*, pages 834–843, 2021.
- [56] Enze Xie, Wenhai Wang, Zhiding Yu, Anima Anandkumar, Jose M Alvarez, and Ping Luo. Segformer: Simple and efficient design for semantic segmentation with transformers. *Advances in Neural Information Processing Systems*, 34:12077–12090, 2021.
- [57] Qi Xu, Liang Yao, Zhengkai Jiang, Guannan Jiang, Wenqing Chu, Wenhui Han, Wei Zhang, Chengjie Wang, and Ying Tai. Dirl: Domain-invariant representation learning for generalizable semantic segmentation. In *Proceedings of the AAAI Conference on Artificial Intelligence*, volume 36, pages 2884–2892, 2022.
- [58] Xiang Xu, Xiong Zhou, Ragav Venkatesan, Gurumurthy Swaminathan, and Orchid Majumder. d-sne: Domain adaptation using stochastic neighborhood embedding. In *Proceedings of the IEEE/CVF Conference on Computer Vision and Pattern Recognition*, pages 2497–2506, 2019.
- [59] Fisher Yu, Wenqi Xian, Yingying Chen, Fangchen Liu, Mike Liao, Vashisht Madhavan, and Trevor Darrell. Bdd100k: A diverse driving video database with scalable annotation tooling. *arXiv preprint arXiv:1805.04687*, 2(5):6, 2018.
- [60] Qihang Yu, Huiyu Wang, Dahun Kim, Siyuan Qiao, Maxwell Collins, Yukun Zhu, Hartwig Adam, Alan Yuille, and Liang-Chieh Chen. Cmt-deeplab: Clustering mask transformers for panoptic segmentation. In *Proceedings of the IEEE/CVF Conference on Computer Vision and Pattern Recognition*, pages 2560–2570, 2022.
- [61] Qihang Yu, Huiyu Wang, Siyuan Qiao, Maxwell Collins, Yukun Zhu, Hartwig Adam, Alan Yuille, and Liang-Chieh Chen. k-means mask transformer. In *Computer Vision–ECCV 2022: 17th European Conference, Tel Aviv, Israel, October 23–27, 2022, Proceedings, Part XXIX*, pages 288–307. Springer, 2022.
- [62] X. Yue, Y. Zhang, S. Zhao, A. Sangiovanni-Vincentelli, K. Keutzer, and B. Gong. Domain randomization and pyramid consistency: Simulation-to-real generalization without accessing target domain data. In *Proceedings of the IEEE/CVF International Conference on Computer Vision (ICCV)*, pages 2100–2110, 2019.
- [63] Xiangyu Yue, Yang Zhang, Sicheng Zhao, Alberto Sangiovanni-Vincentelli, Kurt Keutzer, and Boqing Gong. Domain randomization and pyramid consistency: Simulation-to-real generalization without accessing target domain data. In *Proceedings of the IEEE/CVF International Conference on Computer Vision*, pages 2100–2110, 2019.
- [64] Shanshan Zhao, Mingming Gong, Tongliang Liu, Huan Fu, and Dacheng Tao. Domain generalization via entropy regularization. *Advances in Neural Information Processing Systems*, 33:16096–16107, 2020.
- [65] Yuyang Zhao, Zhun Zhong, Na Zhao, Nicu Sebe, and Gim Hee Lee. Style-hallucinated dual consistency learning for domain generalized semantic segmentation. In *Computer Vision–ECCV 2022: 17th European Conference, Tel Aviv, Israel, October 23–27, 2022, Proceedings, Part XXVIII*, pages 535–552. Springer, 2022.
- [66] Zhun Zhong, Yuyang Zhao, Gim Hee Lee, and Nicu Sebe. Adversarial style augmentation for domain generalized urban-scene segmentation. In *Advances in Neural Information Processing Systems*, 2022.
- [67] Kaiyang Zhou, Yongxin Yang, Timothy Hospedales, and Tao Xiang. Learning to generate novel domains for domain generalization. In *European conference on computer vision*, pages 561–578. Springer, 2020.
- [68] Xizhou Zhu, Weijie Su, Lewei Lu, Bin Li, Xiaogang Wang, and Jifeng Dai. Deformable detr: Deformable transformers for end-to-end object detection. In *International Conference on Learning Representations*, 2021.

Table 7: Performance comparison of the proposed CMFormer vs. existing domain generalized USSS methods when use the VGG-16 as backbones. The symbol '-' indicates cases where the metric is either not reported or the official source code is not available. Evaluation metric mIoU is given in (%).

Method	Proc. & Year	Trained on GTA5 (G)				Trained on SYNTHIA (S)				Trained on Cityscapes (C)			
		→ C	→ B	→ M	→ S	→ C	→ B	→ M	→ G	→ B	→ M	→ G	→ S
IBN [35]	ECCV2018	31.25	31.68	33.27	26.45	31.68	28.34	29.97	26.03	45.55	53.63	43.64	24.78
IW [36]	CVPR2019	35.70	27.11	27.98	26.65	28.00	26.80	24.70	25.82	45.37	53.02	42.79	23.97
Itemnorm [17]	CVPR2019	-	-	-	-	-	-	-	-	-	-	-	-
DRPC [62]	ICCV2019	36.11	31.56	32.25	26.89	35.52	29.45	32.27	26.38	46.86	55.83	43.98	24.84
ISW [7]	CVPR2021	34.36	33.68	34.62	26.99	36.21	31.94	31.88	26.81	47.26	54.21	42.08	24.92
GTR [37]	TIP2021	36.10	32.14	34.32	26.45	36.07	31.57	30.63	26.93	45.93	54.08	43.72	24.13
DURL [57]	AAAI2022	-	-	-	-	-	-	-	-	-	-	-	-
SHADE [65]	ECCV2022	-	-	-	-	-	-	-	-	-	-	-	-
SAW [38]	CVPR2022	38.21	36.30	36.87	28.45	38.36	34.32	33.23	27.94	49.19	56.37	45.73	26.51
WildNet [23]	CVPR2022	39.18	34.49	40.75	27.25	-	-	-	-	-	-	-	-
AdvStyle [66]	NeurIPS2022	-	-	-	-	-	-	-	-	-	-	-	-
CMFormer (Ours)	2023	55.31	49.91	60.09	43.80	44.59	33.44	43.25	40.65	59.27	71.10	58.11	40.43
		↑16.13	↑13.61	↑19.34	↑15.35	↑6.23	↓0.88	↑10.02	↑12.71	↑10.08	↑14.73	↑12.38	↑13.92

Table 8: Performance comparison of the proposed CMFormer vs. existing domain generalized USSS methods when use the ResNet-101 as backbones. The symbol '-' indicates cases where the metric is either not reported or the official source code is not available. Evaluation metric mIoU is given in (%).

Method	Proc. & Year	Trained on GTA5 (G)				Trained on SYNTHIA (S)				Trained on Cityscapes (C)			
		→ C	→ B	→ M	→ S	→ C	→ B	→ M	→ G	→ B	→ M	→ G	→ S
IBN[35]	ECCV2018	37.42	38.28	38.28	28.69	34.18	32.63	36.19	28.15	50.22	58.42	46.33	27.57
IW [36]	CVPR2019	36.11	36.56	32.59	28.43	31.60	35.48	29.31	27.97	50.10	56.16	45.21	27.18
Itemnorm [17]	CVPR2019	-	-	-	-	-	-	-	-	-	-	-	-
DRPC [62]	ICCV2019	42.53	38.72	38.05	29.67	37.58	34.34	34.12	29.24	51.49	58.62	46.87	28.96
ISW [7]	CVPR2021	42.87	38.53	39.05	29.58	37.21	33.98	35.86	28.98	50.98	59.70	46.28	28.43
GTR [37]	TIP2021	43.70	39.60	39.10	29.32	39.70	35.30	36.40	28.71	51.67	58.37	46.76	29.07
DURL [57]	AAAI2022	-	-	-	-	-	-	-	-	-	-	-	-
SHADE [65]	ECCV2022	46.66	43.66	45.50	-	-	-	-	-	-	-	-	-
SAW [38]	CVPR2022	45.33	41.18	40.77	31.84	40.87	35.98	37.26	30.79	54.73	61.27	48.83	30.17
WildNet [23]	CVPR2022	45.79	41.73	47.08	32.51	-	-	-	-	-	-	-	-
AdvStyle [66]	NeurIPS2022	43.44	40.32	41.96	-	39.74	28.33	32.87	-	-	-	-	-
CMFormer (Ours)	2023	55.31	49.91	60.09	43.80	44.59	33.44	43.25	40.65	59.27	71.10	58.11	40.43
		↑8.65	↑6.25	↑13.01	↑11.29	↑3.72	↓2.54	↑5.99	↑9.86	↑4.54	↑9.83	↑9.28	↑10.26

6 More Comparison with State-of-the-art from Other Backbones

In addition to Table 1 in the main submission, which compares the proposed CMFormer with existing CNN based domain generalized USSS methods using ResNet-50 backbone, here we provide further comparison with other backbones such as VGG-16 [46] and ResNet-101 [14].

Results on VGG-16 Table 7 reports the results of existing domain generalized USSS methods on the VGG-16 backbone and comparison with the proposed CMFormer. Under the $G \rightarrow C, B, M, S$ setting, the proposed CMFormer outperforms second-best by 16.13%, 13.61%, 19.34% and 15.34%, respectively. Under the $S \rightarrow C, B, M, G$ setting, the proposed CMFormer outperforms second-best by 6.23% on C, 10.02% on M, and 12.71% on G, respectively. The reason for the slightly inferior performance against SAW [38] by 0.88% on B has been discussed in our submission, as S source domain has small amount of training samples for ViT models. Under the $C \rightarrow B, M, G, S$ setting, the proposed CMFormer outperforms the second-best by 10.08%, 14.73%, 12.38% and 13.92%, respectively.

Results on ResNet-101 Table 8 reports the results of existing domain generalized USSS methods on the ResNet-101 backbone and comparison with the proposed CMFormer. Under the $G \rightarrow C, B, M, S$ setting, the proposed CMFormer outperforms the second-best by 8.65%, 6.25%, 13.01% and 11.29%, respectively. Under the $S \rightarrow C, B, M, G$ setting, the proposed CMFormer outperforms the second-best by 3.72%, 5.99% and 9.86% on C, M, G, respectively. On B, the performance is 2.54% inferior to SAW [38]. Under the $C \rightarrow B, M, G, S$ setting, the proposed CMFormer outperforms the second-best by 10.08%, 14.73%, 12.38% and 13.92%, respectively.

7 Model-size vs. Performance

We validate the trade-off between model size and performance. Specifically, under the C→S setting, the parameters (denoted as para. num.) and GFLOPs of existing CNN based methods are compared with the proposed CMFormer. In addition, we report the results of the proposed CMFormer under the Swin-Tiny, Swin-Base and Swin-Large backbones respectively for more comprehensive comparison. Table 9 summarizes these statistics, and Fig. 8 visualizes them. Some important observations can be made.

(1) When using the Swin-Tiny backbone, the proposed CMFormer shows its superiority on both segmentation accuracy and computational efficiency against existing CNN based domain generalized USSS methods. It shows a 8.93% mIoU against ISW [7] with an even 60.63 less GFLOPs.

(2) The use of Swin-Base backbone can double both the GFLOPs and parameter number of the proposed CMFormer, when compared with existing CNN based domain generalized USSS methods. However, an additional 5.30% mIoU against the Swin-Tiny backbone can be gained, leading to a total of 14.23% mIoU improvement against the CNN based ISW [7].

(3) The use of Swin-Large backbone can double both the GFLOPs and parameter number of the proposed CMFormer compared with the use of Swin-Base backbone. However, this huge computational cost only leads to an additional performance gain of 2.52% mIoU. Thus, the use of Swin-Base backbone seems to be a good trade-off between model size and segmentation accuracy.

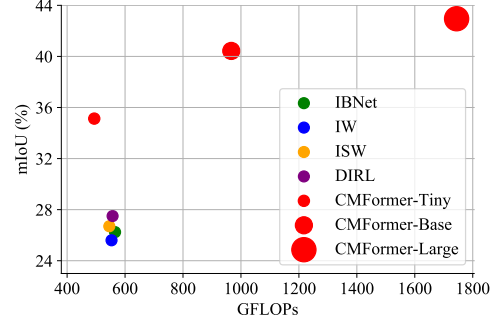


Figure 8: Visualization of mIoU (y-axis in %) vs. GFLOPs (x-axis) of existing domain generalized USSS methods and the proposed CMFormer.

Table 9: Comparison of parameter number, GFLOPs and mIoU of the proposed CMFormer with some existing CNN based domain generalized methods under the C→S setting.

Method	Backbone	GFLOPs	Para. num.	mIoU (%)
IBN [35]	ResNet-50	554.31	45.08	26.14
IW [36]		554.31	45.08	26.10
ISW [7]		554.31	45.08	26.20
DURL [57]		554.98	45.41	26.50
CMFormer	Swin-Tiny	493.68	48.30	35.13
	Swin-Base	966.65	110.59	40.43
	Swin-Large	1744.28	221.18	42.95

8 Effectiveness on Generic Domain Generalization

Following the prior domain generalized USSS work AdvStyle [66], We also test if the proposed content-enhanced strategy can be scalable to generic domain generalization. Two commonly-used benchmarks for generic domain generalization are Digits¹ and PACS², respectively. Existing state-of-the-art generic domain generalization methods, namely, ERM [49], CCSA [32], d-SNE [58], JiGen [1], ADA [50], M-ADA [41], ME-ADA [64], RSC [18] and L2D [55], are involved for comparison. As the proposed content-enhanced strategy is designed for Transformer architectures, we choose ViT-Tiny based L2D pipeline as our baseline. Then, we embed the proposed content-enhanced strategy into the baseline (denoted as L2D+CE), and report its performance on these settings.

Results on Digits Dataset The results are reported in Table 10. The proposed content-enhanced strategy leads to a performance gain of 1.1%, 0.8% and 2.2% under the SVHN, MNIST-M and USPS target domain respectively, when compared with the ViT-tiny based L2D baseline. Also, on the USPS target domain, it achieves the state-of-the-art performance with an accuracy of 82.4%.

¹<http://yann.lecun.com/exdb/mnist/>

²<http://sketchx.eecs.qmul.ac.uk/>

Results on PACS Dataset The results are reported in Table 11. Different from Digits dataset, the evaluation protocol of PACS dataset requires using Art., Car., Ske. and Pho. as the source domain, and reports the average accuracy of the rest three target domains. The proposed content-enhanced strategy leads to a performance gain of 0.6%, 0.8%, 0.5% and 0.7% against the ViT-tiny based L2D baseline, when using Art., Cars., Ske., and Pho. as the source domain, respectively. Noticeably, it achieves the state-of-the-art performance on PACS dataset.

Table 10: Experiments of generic domain generalization on Digits dataset. MNIST is used as source domain. From the third to fifth column, the results on the SVHN, MNIST-M and USPS target domain are reported. Metric accuracy is presented in (%).

Method	backbone	SVHN	MNIST-M	USPS
ERM [49]	LeNet	27.8	52.7	76.9
CCSA [32]	LeNet	25.9	49.3	83.7
d-SNE [58]	ResNet-18	26.2	51.0	93.2
JiGen [1]	ResNet-18	33.8	57.8	77.2
ADA [50]	LeNet	35.5	60.4	77.3
M-ADA [41]	LeNet	42.6	67.9	78.5
ME-ADA [64]	LeNet	42.6	63.3	81.0
L2D	ViT-tiny	41.1	55.3	80.2
L2D + CE	ViT-tiny	42.2	56.1	82.4
		↑1.1	↑0.8	↑2.2

Table 11: Experiments of generic domain generalization on PACS dataset. Art., Car., Ske. and Pho. is used as the source domain respectively, from the third to sixth column. The average accuracy on the rest three target domains is reported in (%).

Method	Backbone	Art.	Car.	Ske.	Pho.	avg.
ERM [49]	LeNet	67.4	74.4	51.4	42.6	58.9
JiGen [1]	ResNet-18	69.1	74.6	52.4	41.5	59.4
RSC [18]	ResNet-18	68.8	74.5	53.6	41.9	59.7
L2D [55]	ResNet-18	74.3	77.5	54.4	45.9	63.0
L2D	ViT-tiny	74.8	77.2	54.5	48.6	63.7
L2D + CE	ViT-tiny	75.4	78.0	55.0	49.3	64.4
		↑0.6	↑0.8	↑0.5	↑0.7	↑0.7

9 More Visualized Results

Following Sec.4.6 in the main submission, more visual results under the $C \rightarrow B, M, G, S$ setting and under the $C \rightarrow$ adverse domain setting are provided in Fig. 9 and Fig. 10, respectively. It can be seen that, under a variety of urban styles and adverse domains like rain, fog and snow, the proposed CMFormer shows a more precise and more reasonable inference than existing CNN based domain generalized USSS methods.

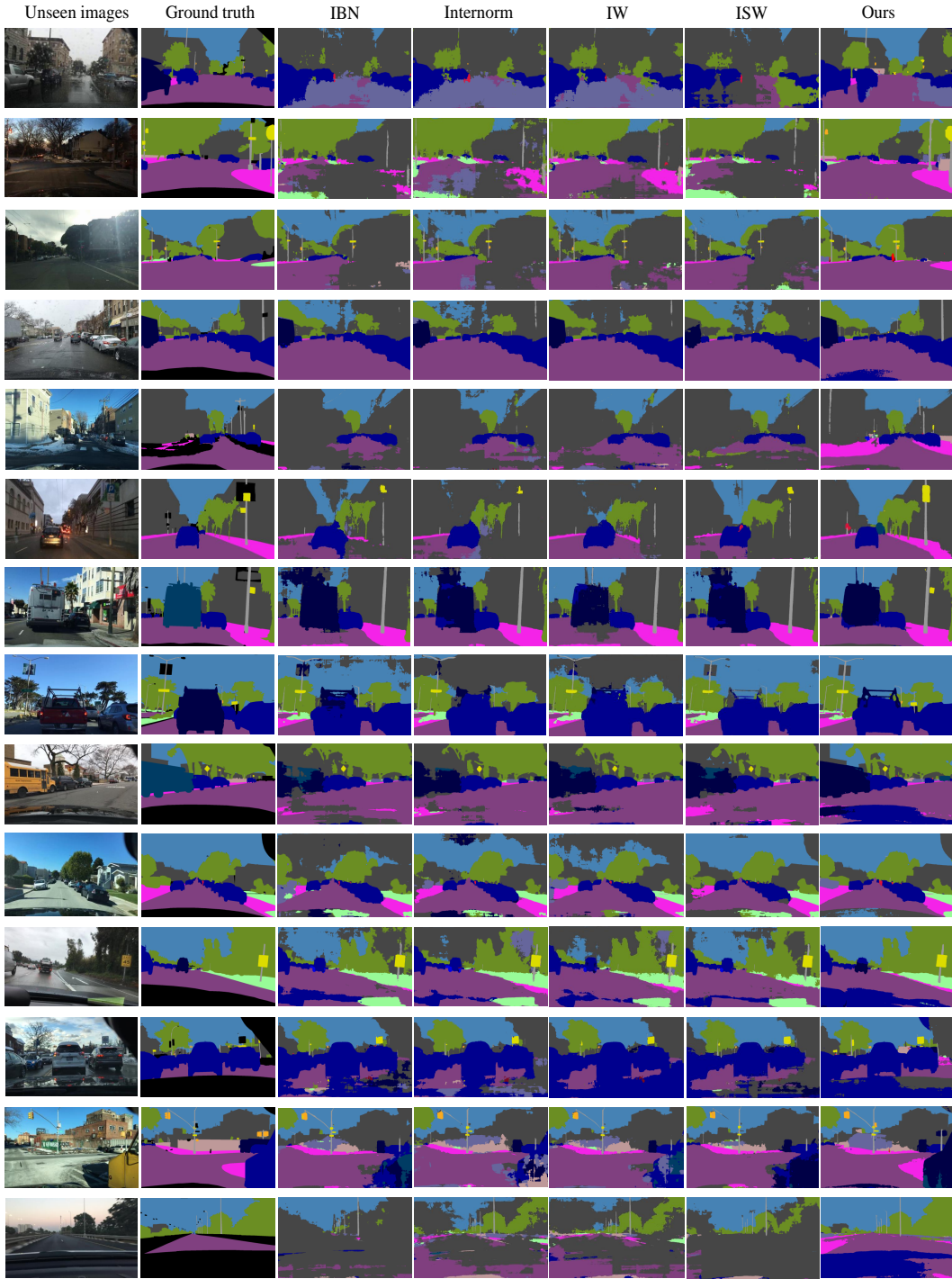


Figure 9: Visualized results of existing domain generalized USSS methods (IBN [35], IW [36], Internorm [17], ISW [7]) and the proposed CMFormer under the $C \rightarrow B, M, G, S$ setting. The proposed CMFormer shows a significantly better inference than existing methods.

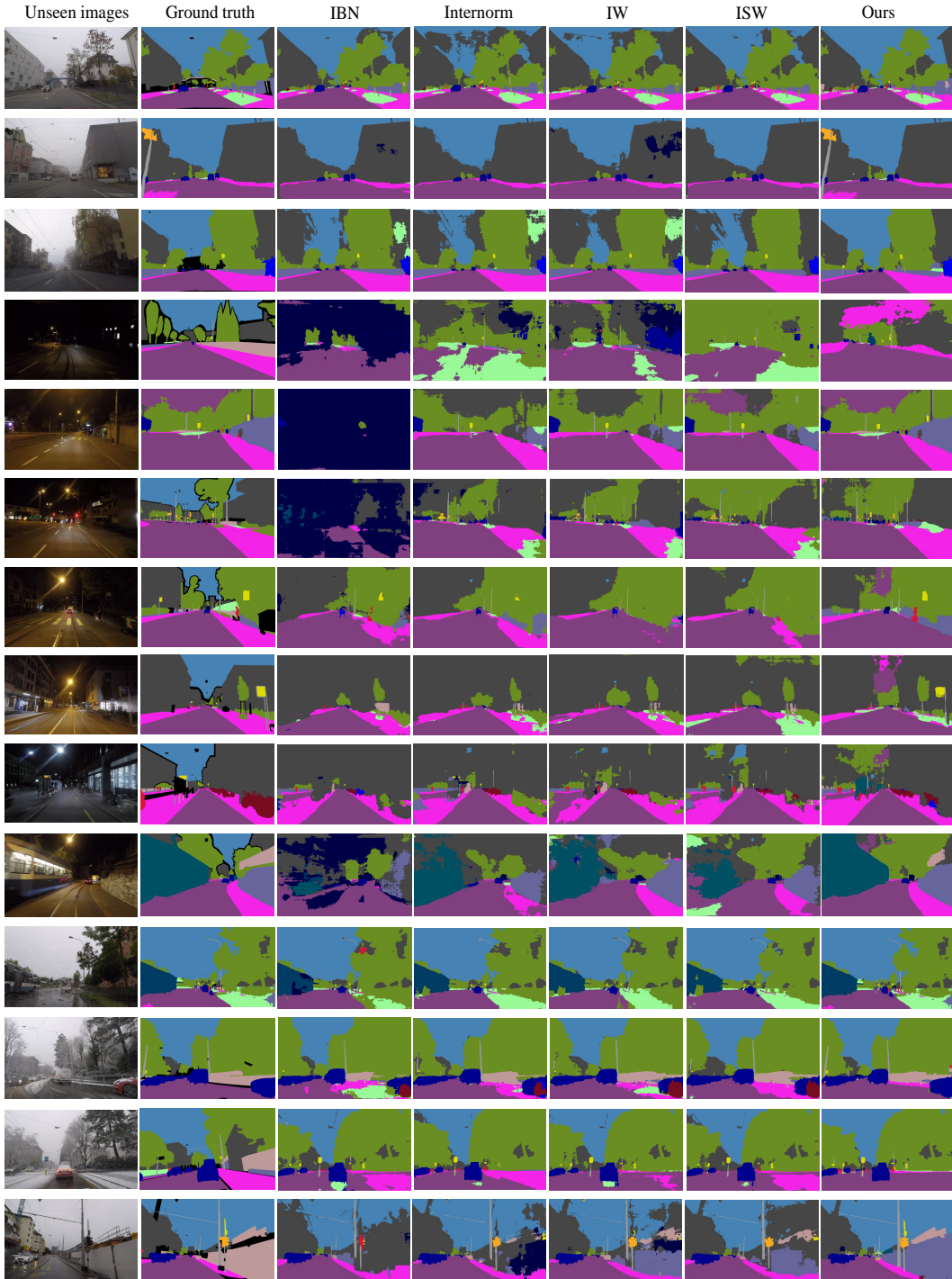


Figure 10: Visualized results of existing domain generalized USSS methods (IBN [35], IW [36], Internorm [17], ISW [7]) and the proposed CMFormer under the $C \rightarrow$ adverse domain setting. The proposed CMFormer shows a significantly better inference than existing methods.